Process parameters investigation for direct powder bed selective laser processing of silicon carbide parts

Alejandro Montón Zarazaga, Mohamed Abdelmoula, Gökhan Küçüktürk, Francis Maury, Marc Ferrato, David Grossin

Progress in Additive Manufacturing (2022) 7:1307–1322
https://doi.org/10.1007/s40964-022-00305-7

FULL RESEARCH ARTICLE

Process parameters investigation for direct powder bed selective laser processing of silicon carbide parts

Alejandro Montón Zarazaga[1] · Mohamed Abdelmoula[2] · Gökhan Küçüktürk[2] · Francis Maury[1] · Marc Ferrato[3] · David Grossin[1]

Received: 28 October 2021 / Accepted: 27 March 2022 / Published online: 19 May 2022

Abstract
Direct-powder bed selective laser processing (D-PBSLP) is a promising technique for the manufacturing of complex-shaped parts of Silicon Carbide (SiC) ceramic. In this work, a complex optimization of the process parameters was performed by numerical and experimental analysis. The numerical model was used to determine and optimize the effect of laser power, scanning speed and hatching distance at different layer thicknesses of 20, 30 and 40 µm. Regarding the experimental process parameters study, powder compaction was also studied and optimized. The optimization parameter criteria were to achieve reproducible and high relative density parts. Concerning the experimental manufacturing process, D-PBSLP of alpha-silicon carbide parts with a maximum relative density of 81% were manufactured. Moreover, the process viability can be confirmed with the manufacturing of SiC complex shapes in absence of any additives in the initial powder and without or post-treatment. The results from this study could be used as a guide for process parameters selection.

Keywords Silicon carbide · Selective laser sintering/melting · Simulation · Ceramic · Additive manufacturing

1 Introduction

Silicon Carbide (SiC) is considered an important ceramic material with a wide range of applications because of its unique characteristics. These excellent properties include high mechanical stiffness, low density, wide bandgap, low coefficient of thermal expansion, high thermal stability, and resistance to corrosive environments [1]. Among SiC applications, this ceramic material is used for high-temperature electronics/optics for automotive, laser processes mirrors and well-logging, and high-power microwave devices for commercial and military systems. Also, SiC is used in electronic devices (LED's, MOSFET's), rugged MEMSs (micro-electro- mechanical sensors) devices for hostile environments, gas and chemical sensors for internal combustion engines, furnaces, and boilers; solar-blind UV photodetectors [2], very high temperature solar absorber [3] and aerospace applications as space telescope mirrors [4] and more generally very large telescopes [5, 6]. Specifically, some of these applications need complex design which can hardly be achieved by using conventional manufacturing methods. In this regard, Additive Manufacturing (AM), which is a developing manufacturing technology that can produce parts from 3D model layer upon layer as defined by ISO/ASTM 52900, can offer a great opportunity to overcome the manufacturing of complex parts and other manufacturing limits.

There are different techniques that can be used for AM of SiC, such as Robocasting [7], Photopolymerization [8], Binder jetting [9], and Powder Bed Selective Laser Processing (PBSLP) [10], among others. Specifically, SiC can be manufactured by AM following direct and indirect approaches [11]. Direct method means that no debinding and post-sintering steps are required while indirect approach uses an initial powder mixture of SiC powder with other additives such as polymer to act as a binder [12, 13].

Regarding some works in indirect AM methods, Chen et al. [14] used a SiC ceramic green body which was prepared by gel casting method and light-curing additive

✉ Alejandro Montón Zarazaga
alejandro.montonzarazaga@ensiacet.fr

[1] CIRIMAT, Université de Toulouse, CNRS, INP-ENSIACET, 4 Allée Émile Monso, 31432 Toulouse Cedex 4, France

[2] Department of Mechanical Engineering, Gazi University, Ankara 06500, Turkey

[3] Mersen Boostec, Zone Industrielle Bazet ouest, 65460 Bazet, France

manufacturing. The results showed that the addition of 1 wt.% PEG and 4 wt.% sucrose can improve the surface quality and sintered body properties of SiC ceramics by this method. Cai et al. [7] fabricated geometrically complex and three-dimensional (3-D) structures of SiC by robocasting, followed by low-pressure spark plasma sintering (SPS) to produce dense ceramic bodies. A concentrated, aqueous colloidal ink consisting of SiC, Al_2O_3, and Y_2O_3 particles in a dilute polymer solution with a total solids volume fraction of 0.44 was developed to have pseudoplastic behaviour with yield stress rheology. Bai et al. [8] prepared SiC ceramic by stereolithography additive manufacturing combined with different sintering approaches, including liquid phase sintering (LPS), precursor infiltration and pyrolysis (PIP), and liquid silicon infiltration (LSI). Jin et al. [13] combined selective laser sintering (SLS), cold isostatic pressing (CIP) and polymer infiltration pyrolysis (PIP), to manufacture complex silicon carbide parts. The powder used for the selective laser sintering was a mixture of SiC powder and epoxy resin 3 wt.%. However, during the process of degreasing, some carbon was left in the specimen since the resin was carbonized. Liu et al. [12] combined selective laser sintering (SLS), cold isostatic pressing (CIP) and reaction sintering (RS). In the process of LS/CIP/RS, Phenol formaldehyde resin (PF)-SiC composite powder was prepared by mechanical mixing and cold coating methods, with an optimized content of PF at 18 wt.%. To obtain improved density of the sintered body after final reaction sintering, carbon black was added into the initial mixed powder. Song et al. [15] combined reaction-bonded (RB) process and selective laser sintering (SLS) method to find efficient ways to improve the performance of SiC/Si composites prepared by these techniques. Effects of epoxy resin binder on the performance and microstructure of preforms and sintered bodies were studied first. Then, based on the results, graphite with low reactivity was used as an alternative slow-release carbon source to promote sintering densification process and improve the carbon density of preforms. However, regarding indirect AM methods, some problems such as crack formation, shrinkage and slumping can occur due to the debinding and post-sintering processes [16].

On the other hand, indirect AM of SiC powder-bed methods are mainly used. Table 1 shows some previous direct AM studies which were following different strategies. Birmingham et al. [17] achieved direct PBSLP of SiC by scanning silicon (Si) powder in an acetylene (C_2H_2) chamber where silicon carbide could be formed by the reaction of Si with the carbon in the atmosphere. However very porous ceramic parts, with high SiC content, were obtained. To increase the density of the final SiC part by indirect PBSLP, Hon et al.

Table 1 Summary of the process conditions and properties of the SiC manufactured by the PBSLP process

Reference	Year	Powder feedstock	Laser and strategy	Post-treatments	Properties of processed parts[a]
Birmingham et al. [17]	1993	Silicon powder + C_2H_2 Precursor gas	Laser: CO_2 Laser Power: 1.8–2.8 W Scan speed: 500 µm/s Hatching Distance: 50 µm	No post- processing	Not determined
Löschau et al. [19]	2000	SiC	Laser: CO_2 Laser power: 45–52 W Scan speed: 200–300 mm/s Layer Thickness: 50 µm Atmosphere: Argon/air mixture	Liquid Si Infiltration	Mass density: 2.65 g/cm^3 Bending strength: 195 MPa Young's modulus: 225 GPa Thermal expansion coefficient: $40 \cdot 10^{-7}$ K^{-1} Thermal conductivity: 70 W/mK
Hon et al. [18]	2003	50 vol.% polyamide + 50 wt.% SiC	Laser: CO_2 Laser Power: 4–8 W Scan speed: 1000–1250 mm/s Hatching Distance: 0.15–0.0.2 mm Layer Thickness: 0.1–0.125 m	No post-processing	Tensile strength = 46 MPa Young modulus = 2200 MPa
Meyers et al. [16]	2018	Silicon 40%. vol + SiC powder 60% vol	Laser: Fiber Laser Laser Power: 12–21 W Scan speed: 50–500 mm/s Hatching Distance: 77 µm Layer Thickness: 30 µm Scanning strategy: Zig-Zag	Phenolic resin infiltration + Curing + Pyrolysis + Liquid Si Infiltration	Full dense body Vickers hardness = 2045 HV Electrical conductivity = 5.3×10^3 S/m Young's modulus = 285 GPa 4-point bending strength = 162 MPa

[a]Values will be given when possible

[18] manufactured SiC/Polyamide composites by blending 50 vol.% polyamide with 50 vol.% SiC. After the PBSLP, the polymer was an integral part of the final product rather than being removed in downstream processes. Nevertheless, the finals parts had poor mechanical properties. In these terms, Löschau et al. [19] used silicon infiltration in complex pure SiC parts to increase the mechanical and thermal properties. Moreover, during this period, different authors developed a micro laser sintering to fabricate SiC ceramics [20, 21] by blending Si and SiC powder beds which were scanned with a q-switched laser. Next, Meyers et al. [16, 22] laser sintered a powder mixture of silicon carbide (SiC) and silicon (Si) powders where the Si melts and re-solidifies to bind the primary SiC particles. Afterwards, these Si-SiC preforms were impregnated with a phenolic resin, which was pyrolyzed yielding porous carbon and transformed into secondary reaction forming SiC when the preforms were infiltrated with molten silicon in the final step. This resulted in fully dense reaction bonded silicon carbide parts with up to 84 vol.% SiC.

This work is focused on direct-PBSLP since this technique enables a single-step AM process for ceramic manufacturing without the need for post-process pyrolysis or post-sintering steps, avoiding undesirable defects inherently generated by indirect methods such as crack formation, shrinkage, and slumping. However, it can be concluded from the described literature review that there is still a real need to study direct-PBSLP of pure SiC to avoid the use of other initial powder mixtures such us Silicon. Moreover, the manufacturing of 3D SiC parts by direct-PBSLP can be considered a challenge, since SiC is a covalent ceramic that does not have a melt phase under normal atmospheric circumstances but instead decomposes into liquid silicon and solid carbon above 2545 °C [17, 23]. Our previous studies [24], 25 were focused on the SiC manufacturing using direct PBSLP by optimizing the process parameters, specific laser power, scanning speed, and scanning strategy. However, other process parameters (hatching distance, layer thickness and powder compaction) have non ignored effects and are important to contribute to the successful direct-PBSLP. Therefore, this paper aimed to investigate the effect and optimize all the process parameters of SiC direct-PBSLP numerically and experimentally. Moreover, the process optimization and viability are confirmed by the manufacturing of complex SiC structures by means of this technique, in absence of binder or other initial powder mixtures, with a final relative density of 81%, a much higher relative density (≥27%) compared to other PBSLP works in absence of post-treatment. This result opens a new manufacturing optimization for the D-PSBLP field since complex SiC parts with such as high final relative density in absence of any additive, binder, or other initial powder mixture have not been manufactured before.

2 Material and methods

2.1 Feedstock

Feedstock materials were provided by the Mersen Boostec Company that includes silicon carbide powder (α-Si with a purity of ≥98.5%, $d_{50}=20$ µm) and SiC circular baseplate ($d=66$ mm) to be used as a baseplate. The particle size distribution was measured on the Mastersizer 3000 (Malvern Panalytical) laser diffraction particle size analyzer. The powder morphology has irregular shape which could induce problems in layer deposition, since this increases inter-particle friction. Commonly powders that are used in laser sintering are usually spherical or at least have rounded edges. However, deposition trails showed that the powder was able to be deposited layer by layer on the 3D printer without any defect or problem.

Also, the flowability was quantified using the dynamic angle of repose, a generally accepted characterization technique to measure flowability of powders and recommended by ASTM as the characterization method for metal powder for AM since the methodology is closer to these AM processing conditions than other techniques [26]. The angle of repose is then obtained as the angle of the rotating powder mass relative to the horizontal plane [27]. This angle was measured using a Hosokawa Micron's Powder Characteristics Tester PT–S. The average angle of repose obtained from this test was $41 \pm 3°$ for the SiC powder which can be considered an acceptable value for the AM process [16, 28].

2.2 Direct-powder bed selective laser processing (D-PBSLP)

The direct-PBSLP experiment was conducted on the Phenix™ Systems ProX® DMP 200 3D printer manufactured by 3D Systems and equipped with a Fiber laser of 300 W maximum power (laser wavelength = 1060 nm, spot size = 70 µm). Laser Power (P) of 30–50 W, scanning speed (v) of 50–500 mm/s, layer thickness of 20 to 40 µm, hatching distance of 8.75–87.5 µm and powder cylinder compaction of 0–100% were used. The scanning strategy followed a zigzag and hexagonal pattern rotated by 90° between layers as recommended from our previous study [25]. The manufactured parts had a dimension of $10 \times 10 \times 5$ mm^3. Inert argon atmosphere was used to prevent oxidation during the process.

2.3 Characterization techniques

The morphology and phase composition of the raw powder material and the manufactured parts was investigated using scanning electron microscopy (SEM, LEO435VP) and X-ray

diffraction (XRD, D8-2 Bruker), using Cu K- alpha radiation (λ = 1.5406 Å) over the 2θ range of 20°–80°. The phase composition was determined by the Rietveld method from XRD patterns with MAUD, following the strategy developed by Hongchao et al. [29]. Densities of SiC manufactured parts were assessed by the geometrical density and Archimedes' method.

3 Numerical procedure

In PBSLP, a laser beam with specific power and scanning speed is used to scan the powder bed. The sintering process of the powder is considered a complex process and a challenge to be mathematically modelled. To model the sintering process of the powder, some assumptions were considered, such as flat surface of the melt pool, uniform heat distribution of the laser source, no change of the powder absorptivity with temperature, and continuous media of the powder layer. All these assumptions were considered during the development of the model.

3.1 Numerical model development

The heat transfer from the laser source to the powder bed can be described by the energy equation (Eq. (1)) according to [30].

$$\rho C_p \frac{\partial T}{\partial t} = \nabla.(\mathrm{k}\nabla \mathrm{T}) + S_h, \tag{1}$$

where ρ, C_p, T, k, t, and S_h are the density, specific heat, temperature, thermal conductivity, time, and the laser heat source, respectively.

A User-Defined Function (UDF) that describes the laser heat source S_h according to [30] (Eqs. (2), (3), and (4)) was developed, compiled, and solved using ANSYS FLUENT 2020R1. The material properties as a function of temperature were taken into consideration according to the powder data sheet provided by Mersen Boostec® and [24] (Table 2) and were used during the development of the UDF.

$$S_h = AI_o\alpha \exp(-2\frac{\left(x - v_x t\right)^2 + \left(y - v_y t\right)^2}{\omega^2} - \alpha z) \tag{2}$$

$$I_o = \frac{2P}{\pi\omega^2} \tag{3}$$

$$\omega = \frac{D_b}{2 \times 2.146}, \tag{4}$$

where A,α, ω, I_o,D_b,v, and t are the powder absorptivity, absorption coefficient, laser characteristic radius, laser intensity, laser beam diameter, scanning speed, and time, respectively. It is worth to mention the laser intensity was calculated based on laser characteristic radius as described in Eq. (3) according to [30]. The absorption coefficient was estimated according to [31].

The initial and boundary conditions used in this study are shown in Fig. 1. There is heat transfer by conduction from the scanned layer to the base plate and from the layer top surface to the surroundings by radiation and convection. Equations (5) and (6) describe these boundary conditions and the initial condition applied to the model. No preheating was applied in this study, i.e., $T_O = 300\mathrm{K}$ in Eq. (6).

$$T(x, y, z)_{t=0} = T_O, \tag{5}$$

$$-k(\frac{\partial T}{\partial z}) = \dot{S}_h - h_{\mathrm{cov}}\left(T_a - T_s\right) - \sigma\epsilon\left(T_a^4 - T_s^4\right), \tag{6}$$

where h_{cov}, σ, and ϵ are the convection coefficient, emissivity, and Stefan-Boltzmann constant, respectively. Also, the UDF was developed to monitor the sintering process based on the calculated temperature, where any region with

Table 2 The thermo-physical properties of SiC used in analysis

Property	Value	Ref
Density, kg/m^3	3210	Mersen Boostec®
Specific heat J/kg K	−0.0005 T2 + 1.2911T + 337.13 ($T \leq 1273.15$) 0.0201T + 1285.9 ($1273.15 < T < 2200$) 1330 ($T > 2200$) (T, temperature in K)	[24]
Thermal conductivity W/m K (T, temperature in K)	0.0002 T2 −0.4427 T + 295.88 ($T \leq 1273.15$) −8E−05T + 5.676, ($1273.15 < T < 2200$) 5.5 ($T > 2200$) (T, temperature in K)	[24]
Sintering point (°C)	<2525	Mersen Boostec®
Emissivity	0.7	
Absorptivity	0.55	Measured

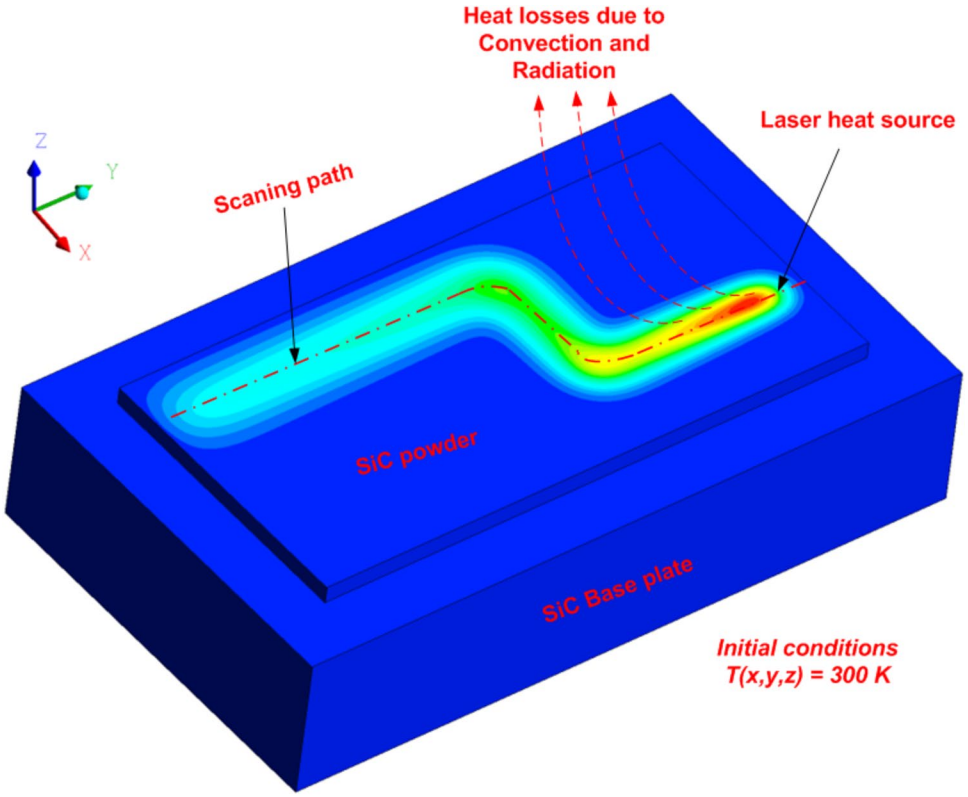

Fig. 1 The initial and boundary conditions applied in the numerical modelling

temperate above the sintering point of SiC is considered a sintered region. This helps to test the used process parameters numerically and see if they can sinter the powder layer or not.

4 Numerical solution methodology

The physical geometry and the computational domain of the model used in the analysis are presented in this section. The validation of the results with the available experimental data is also provided.

4.1 Model geometry

As shown in Fig. 2, the model geometry used in this analysis consists of three parts that represent the base plate, scanned powder layer, and un-scanned powder. It was considered that the powder particles would act as a continuous media. Only one layer was studied in the analysis because it was sufficient to observe the impact of process parameters, and the same behaviour will be replicated in the consecutive layers. The model dimensions are shown in Table 3.

4.2 Numerical solution

ANSYS FLUENT 2020R1 was used to solve the developed numerical model. The process parameters (laser power, scanning speed, layer thickness, and hatching distance) were considered through the UDF which was developed to simulate the sintering process. The computational domain (the mesh), used to solve the model, was created using the ANSYS meshing tool, and very fine discretization was considered for the powder layer as can be seen in Fig. 3. For the un-scanned powder and the baseplate, a bit of coarse discretization was used to reduce the computational time. Figure 4 shows the steps which were followed to solve the developed numerical model. To avoid any inaccurate results coming from low-quality meshing, a mesh density test was carried out. Three different meshes, A, B, and C (Table 4), were investigated regarding the convergence in the obtained results from each mesh. The maximum temperature obtained during scanning was used as a testing criterion. Table 4 summarizes the obtained maximum temperature for each mesh and the maximum temperature for mesh A and B was 2376.3 and 2379.4 K, respectively, with an error of 0.1% between the two values. This means that any discretization after level B will give accurate results and therefore, the mesh C was used for this study. Another two important factors which have a great effect on the accuracy of the obtained results are the time step size and number of iterations per time step.

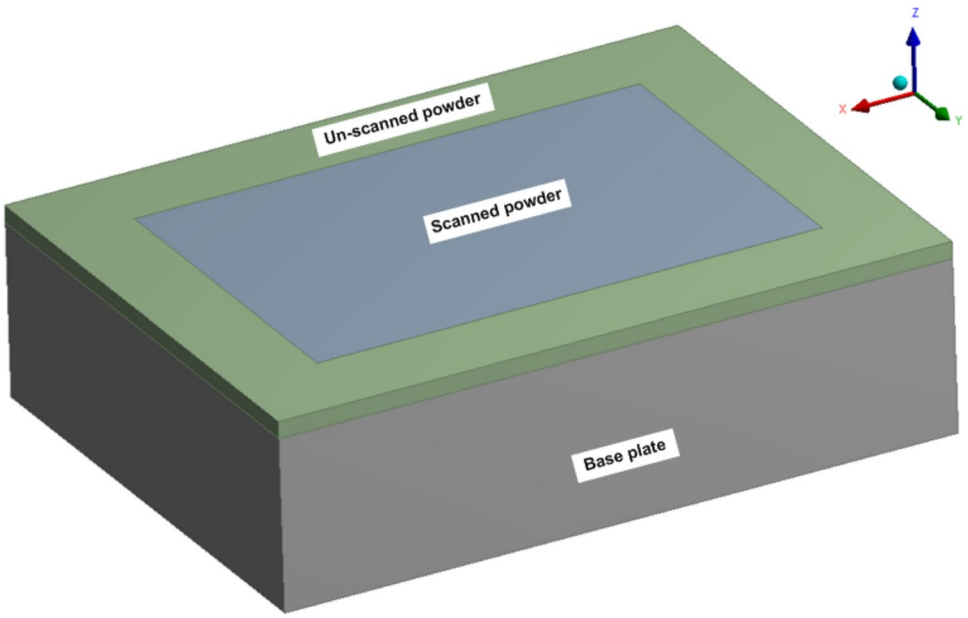

Fig. 2 The model geometry used in the analysis. The un-scanned powder is green, the scanned powder is light grey, and the baseplate is dark grey [not to scale]

Table 3 Model dimensions

Parameter	Base plate	Powder layer
Length (mm)	2.5	2
Width (mm)	1.5	1
Thickness (mm)	0.5	0.02, 0.03 and 0.04

They were considered, selected, and tested to make sure that they did not affect the accuracy of the results. Finally, the results were measured when the temperature history become stable as shown in Fig. 5.

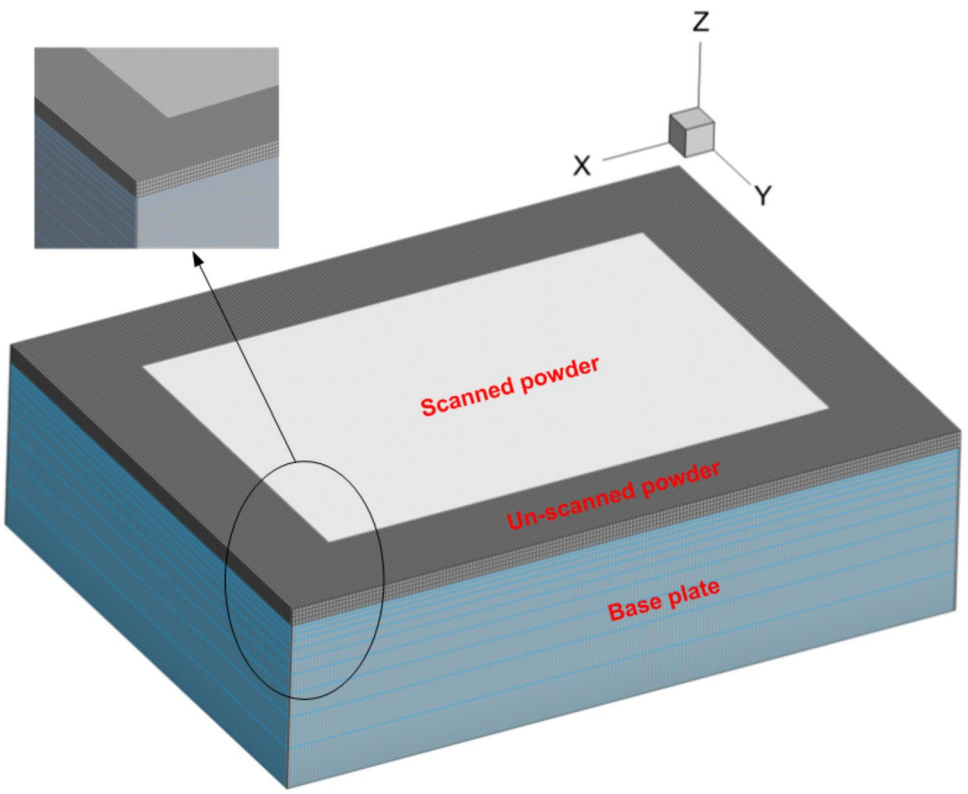

Fig. 3 The computational domain (the mesh) used in the analysis [not to scale]

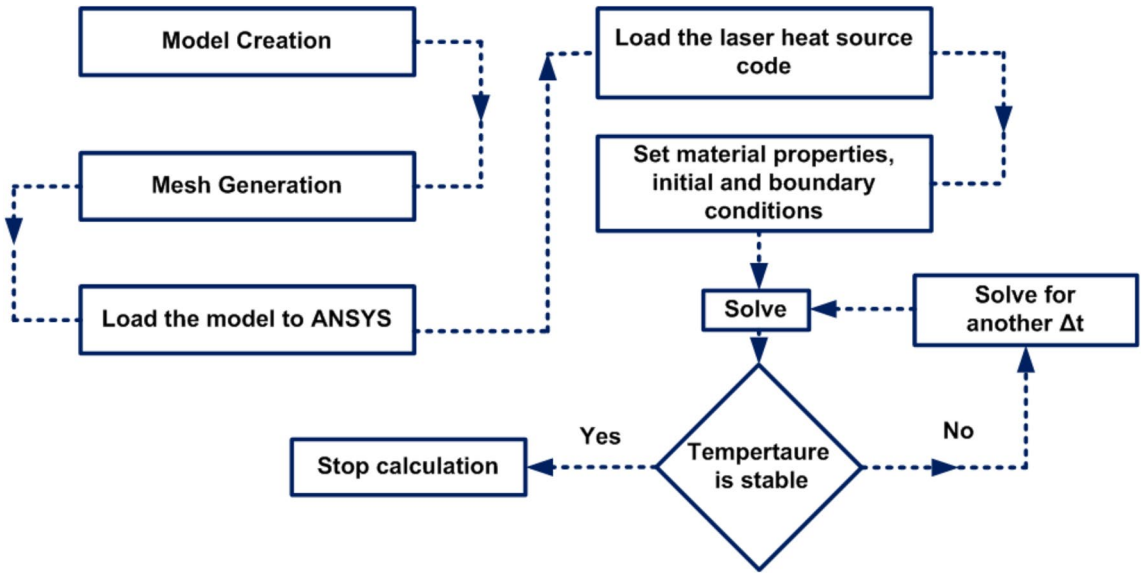

Fig. 4 Numerical procedure flowchart used in this study

Table 4 Meh density analysis

Mesh	Mesh element size (μm)	Number of cores used in the calculation[a]	Elapsed time to solve one time step (s)	Temperature (K)
A	5	48	3.92	2343.7
B	2.5		6.89	2376.37
C	2		8.4	2379.4

[a]2×Intel® Xeon® Gold 6252 Processor (48 cores) is used for calculation with 96 Gb RAM

4.3 Model validation

Validation of the numerical model with experimental results is very important to assure that the model provides similar values to the experimental results. For this purpose, the width and the depth of the scanning path obtained experimentally should be compared with its corresponding values form the numerical model (the width and the depth of scanning path obtained from the numerical model). It was extremely difficult to measure the depth of the scanning path and, therefore, the width of the scanning path, from the numerical model and experimental work, was used for this comparison (Fig. 6a). Different values of laser energy density (LED = laser power/scanning speed) were used in this comparison for different laser power and scanning speed sets (45 W-250 mm/s, 30 W-100 mm/s, 30 W-50 mm/s and

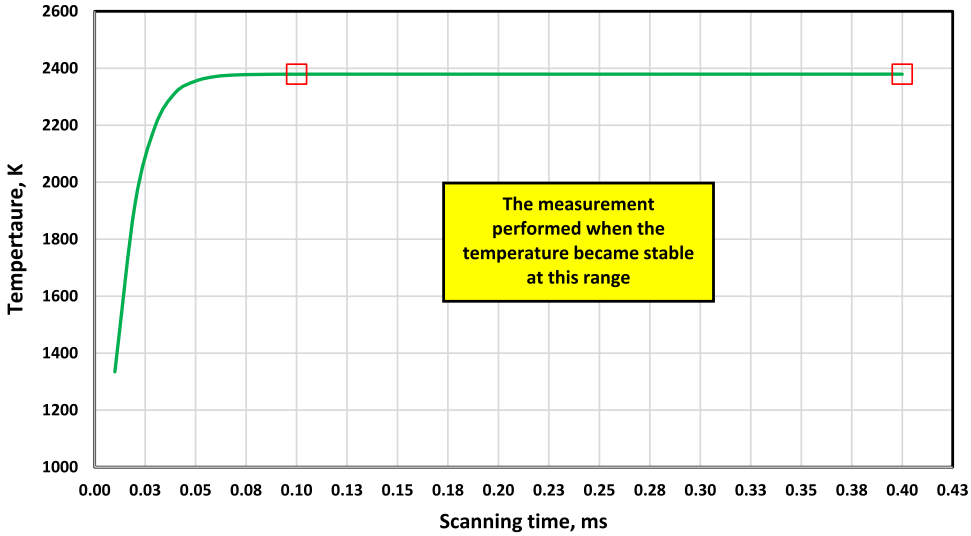

Fig. 5 Temperature history during the scanning process for a line scanning

35 W-100 mm/s). The comparison showed that the developed numerical model and experimental data are in a good agreement, especially at lower LED values where the maximum obtained error is 7.9%. The largest inaccuracy obtained was 13.7% at the higher LED, due to the assumptions considered during the model development (Fig. 6a, b).

To confirm the validation of the numerical model with the experimental results, the temperature distribution of the laser spot obtained from the numerical model, Fig. 6c was compared with experimental data. The experimental temperature of the laser spot was measured using a TVS- 2300ST thermal camera manufactured by Avio Nippon Avionics Co., Ltd. The results indicated that both the numerical and the experimental results provide similar values with a calculation error of 1.24%. It can be concluded that the numerical model gives a similar value compared to the experimental results and can be used as a guide through the experimental work to investigate the process parameters.

5 Results and discussion

The objective of direct-PBSLP was to manufacture SiC parts by using SiC powder as a feedstock in absence of binders, additive or other initial powder mixtures. This can be achieved mainly by using the appropriate process parameters that can manufacture SiC parts without any defects or problems either during or after the process. These process parameters are laser power, scanning speed, hatching distance, layer thickness, and powder compaction. Therefore, this study was focused on investigating and optimizing these process parameters for SiC PBSLP. The numerical model was used to study and optimize the process parameters and provide the appropriate values.

5.1 Numerical results

Regarding the process parameters, any parameters belonging to the laser machine have an influence on the build-up process and, in the end, over the part's relative density. Even if there are many parameters involved, most of the current research on the process optimization have only in consideration the energy density (E_d) or energy input in a defined volume that can be calculated though [32] as follows:

$$E_d = \frac{P_{\text{laser}}}{v_{\text{scan}} \times h_{\text{space}} \times t_{\text{layer}}} \frac{\text{J}}{\text{mm}^3},$$

where E_d is the energy density or energy input in J/mm^3, P_{laser} is the laser power (J/s), v_{scan} the scanning speed (mm/s), h_{space} the hatch distance (mm), and t_{layer} is the powder layer thickness (mm).

Therefore, the numerical model was used to determine the laser power and the scanning speed to obtain a dense structure at different layer thickness. Three following different layer thicknesses were investigated in this study: 20, 30 and 40 µm. For each layer, the recommended laser powers and scanning speeds were calculated form the numerical model. The viability of laser power and scanning speed in direct-PBSLP was evaluated based on three criteria. These three criteria were as follows: (1) whether sintering takes place across the layer thickness of the scanned regions, as shown in Fig. 7a; (2) whether it provides a continuous and smooth scanning path during the process as shown in Fig. 7b; (3) whether the maximum temperature during scanning exceeds the decomposition temperature of SiC.

Based on these three criteria, Fig. 8 gives the laser power range for each scanning speed at different layer thicknesses

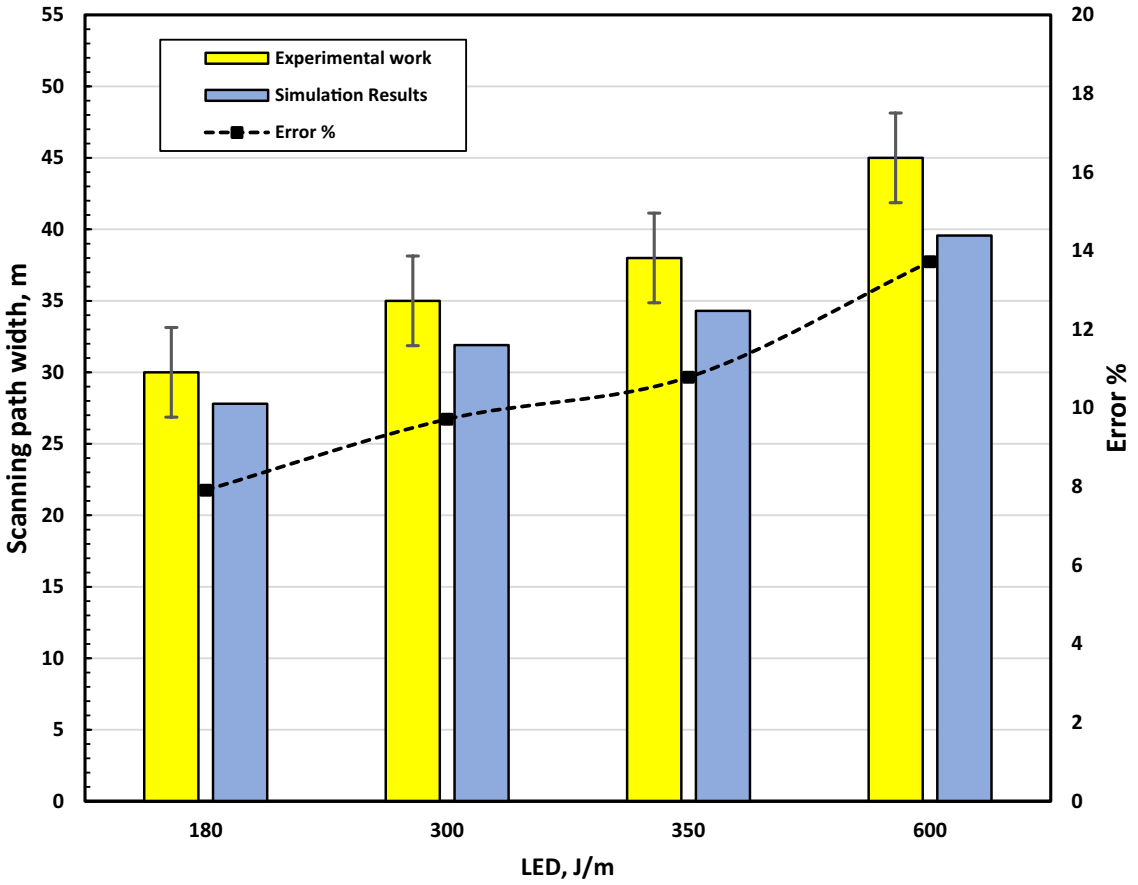

(a)

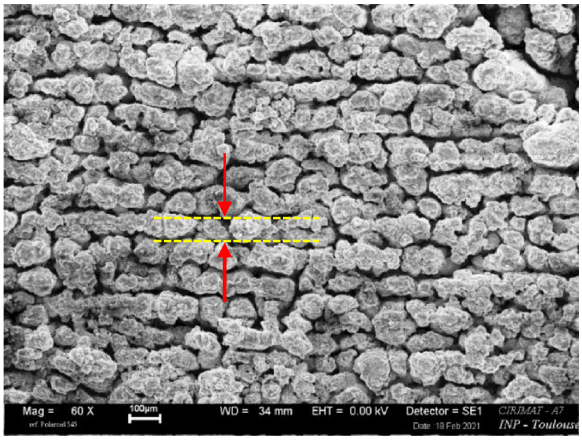

(b)

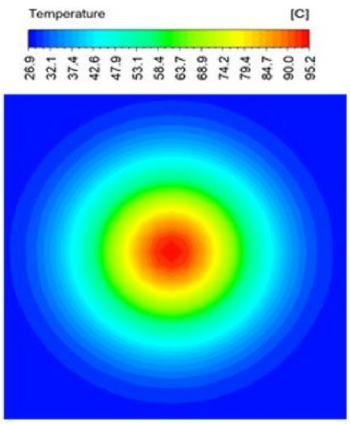

(c)

Fig. 6 **a** Comparison of the scanning path width obtained experimentally with the simulation results at different LEDs, **b** SEM analysis for LED 180 J/m, **c** temperature distribution for the laser spot

in direct-PBSLP of SiC according to the numerical model results. Selected laser power and scanning speeds were experimentally studied and analyzed.

Regarding the hatching distance analysis, which refers to the distance between the centers of adjacent laser beam tracks, during the interaction of the laser beam with the

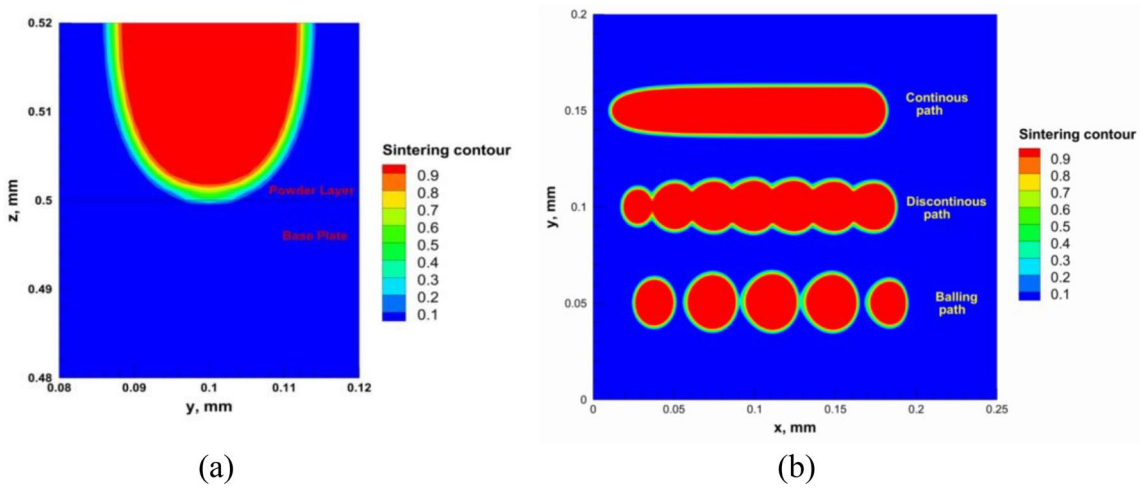

Fig. 7 Criteria on which the laser powers and the scanning speeds were selected

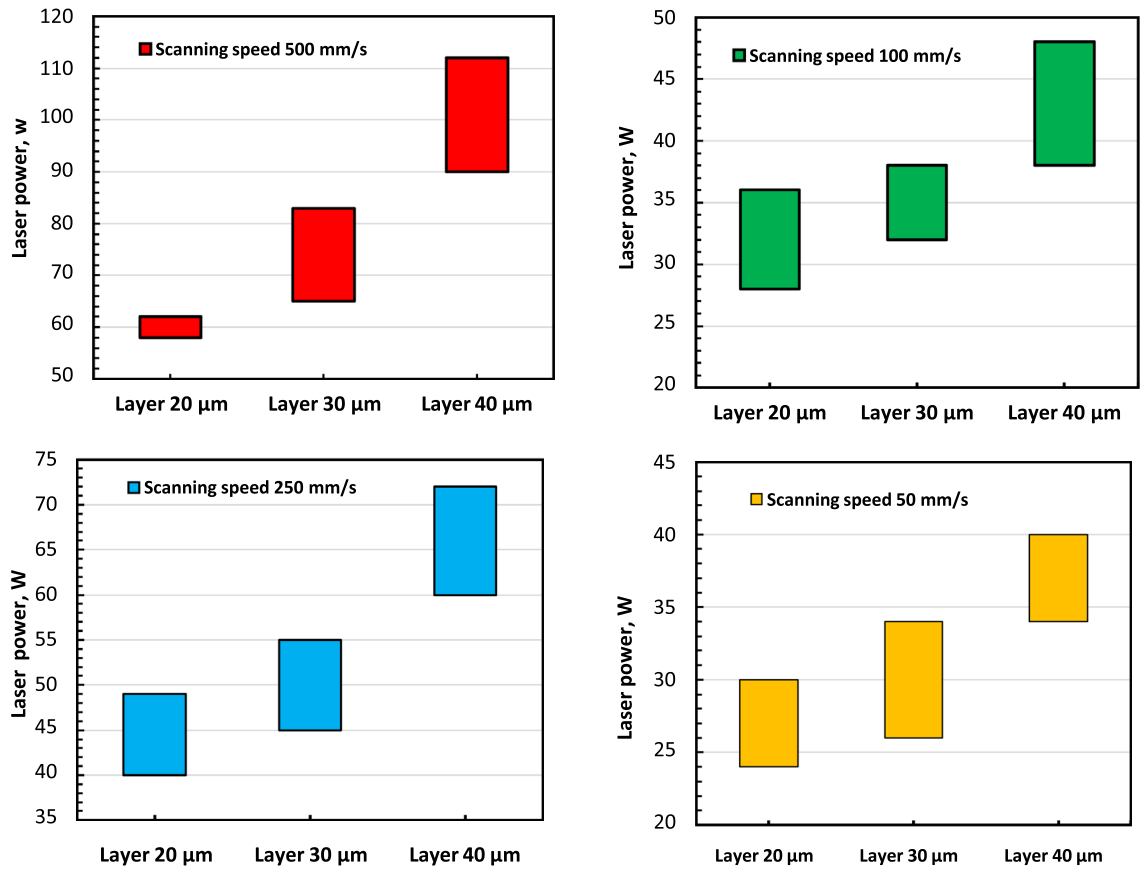

Fig. 8 Laser power and scanning speed values for a different layer thickness

powder feedstock, it is important that the laser traces overlap at a certain rate to avoid insufficient sintering, which may occur due to the absence or insufficient areas of interaction with the laser beam. In this regard, a hatch distance to obtain non-defect reproducible parts and optimized build rate of the process should be considered [10]. Figure 9 shows the sintering contour for different hatching distances (1D, 0.5D, 0.25D, and 0.125D where D is the laser spot size) at the layer top surface. By using hatching distances of 1D and 0.5D, no connection can be observed between the adjacent scanning

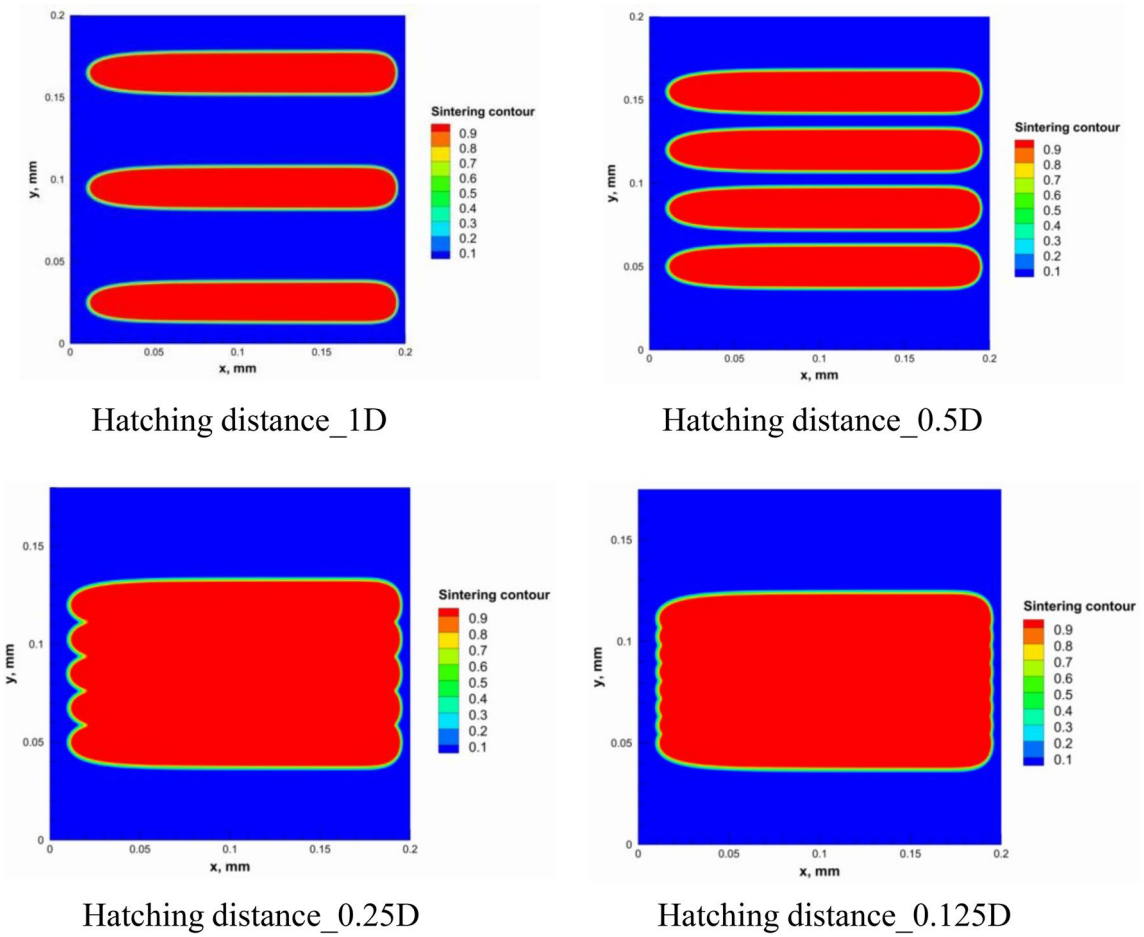

Fig. 9 Sintering contour for different hatching distance

path, which affects the manufactured samples negatively. In consequence for direct-PBSLP of SiC, the hatching distance should not be more than 0.5D (considering the calculation error between the numerical model and the experimental results as described in the model validation). Therefore, hatching distance of 0.5D was used during the experimental work.

5.2 Experimental results

Several SiC parts with a size of $1 \times 1 \times 0.5$ cm^3 were manufactured using the recommended parameter values from the numerical model. It was observed that, SiC parts produced without the combination of the layer thickness and the hatching distance that we described in the previous section, were not reproducible with the addition of the appearance of many defects. In Fig. 10, SiC parts were produced with the following parameters: laser power of 38 W, scanning speed of 100 mm/s, the layer thickness of 30 µm, hatching distance of 0.5D, and zigzag scanning strategy rotated by 90° between layers. The surface morphology was observed by SEM images.

The different patterns between the interior and edges of the parts were obtained due to effect of the scanning strategy. A relative density of $53 \pm 6\%$ was obtained by following the Archimedes' principle. The high porosity is mainly coming due to the use of the maximum laser power value which corresponds to the layer thickness of 30 µm and scanning speed of 100 mm/s as can be seen in Fig. 8. Therefore, it is recommended to use intermediate power values from the guide chart (Fig. 8).

Moreover, in some PBSLP machines, the powder coating unit performs the powder spreading with a rotary cylinder, so the powder is in a compressible state while being laid at the same time. This compression increases the packing density of the powder bed and hence has a direct influence on the final density and quality of the manufactured parts. Thus, to establish which powder compaction is more favourable for the process, the other parameters were kept constant.

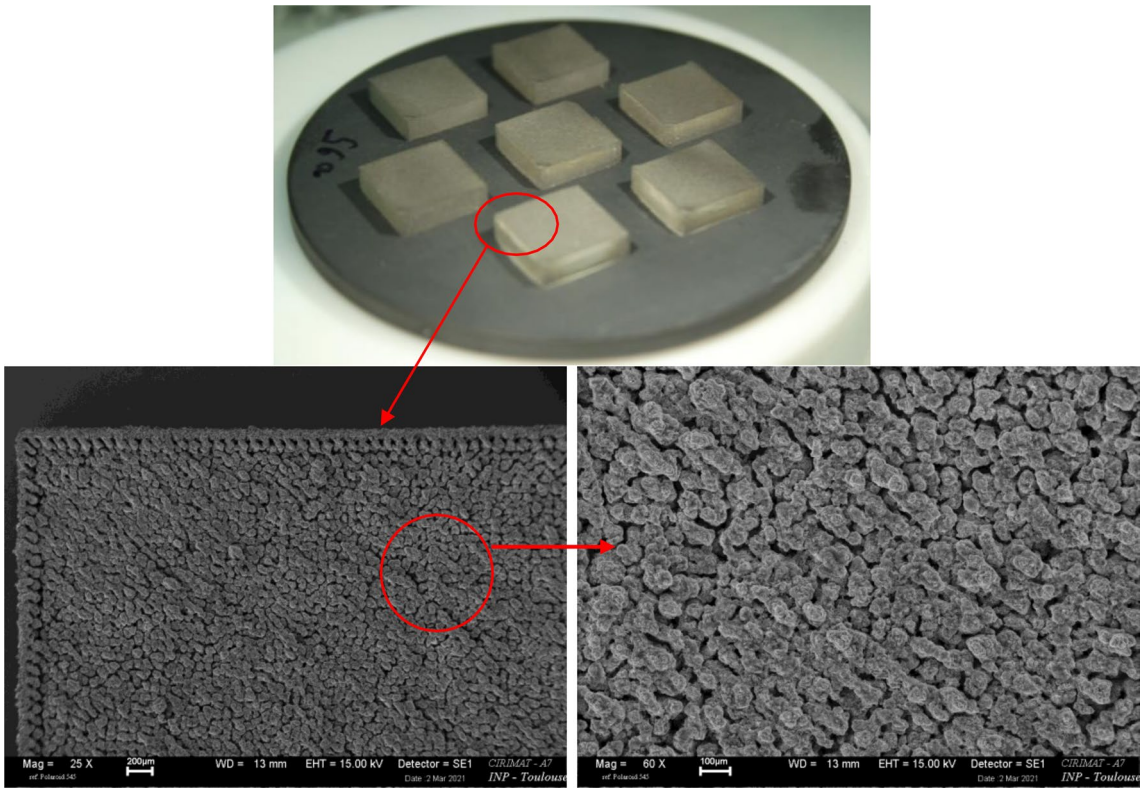

Fig. 10 SiC parts manufactured by PBSLP (10 mm × 10 mm × 5 mm) layer thickness 30 µm and Scan spacing 35 µm

Table 5 Geometrical density measurement of SiC parts by PBSLP with different powder compactions

Powder compaction (%)	Density (g/cm^3)
0	1.4 ± 0.11
50	1.6 ± 0.19
100	1.8 ± 0.08

The geometrical density measurements are given in Table 5 and the best result was achieved using 100% compaction.

Other SiC pieces were manufactured with different PBSLP process parameters following the numerical results. These parameters were laser power: 45 W, scanning speed: 250 mm/s, layer thickness: 30 µm, hatching distance: 35 µm, scanning strategy: hexagonal rotated by 90 degrees between layers, and powder compaction: 100%, respectively. After the PBSLP, the relative density of the part was measured 11

as 81 ± 3% following the Archimedes' principle. Observing the morphology by SEM (Fig. 11), a sintered surface was observed without any characteristic pattern, especially needle-like protrusions in laser track lines due to laser manufacturing. Besides, the formation of microcracks (Fig. 11) was possibly produced due to the thermal shocks generated by the high temperature that was reached by the material–laser interaction.

The numerical model was used to interpret the difference in the relative density for the case 45 W-250 mm/s and 38 W-100 mm/s. For the case 38 W-100 mm/s, the maximum temperature history has reached a temperature above the decomposition limit (Fig. 12); consequently more porosity was formed. For the case 45 W-250 mm/s, the maximum reached temperature was between the sintering and decomposition limit. It was considered that almost no decomposition happened except decomposition due to some pick-up in the temperature inherently caused by the scanning strategy.

In the X-ray diffraction spectrum of the sample (Fig. 13), silicon carbide phases and Si and C elements were observed. Specifically, the analysis result indicates that SiC exhibited four distinct crystalline structure: SiC-6H and SiC-15R like the powder as received, plus carbon (1%) and Silicon (5%) (Table 6). As we indicated, this partial decomposition may occur because of the use of the scanning strategy effect that needs to be investigated in a future study.

Thus, after the optimization of the parameters, to confirm the process viability, the manufacturing of complex shape parts of SiC is possible. The PBSLP parameters were set again at laser power: 45 W, scanning speed: 250 mm/s, layer thickness: 30 µm, hatching distance: 35 µm, scanning strategy: hexagonal rotated by 90 degrees between layers and compaction: 100%, respectively. Figure 14 exhibits a turbine and a lattice structure manufactured with these conditions.

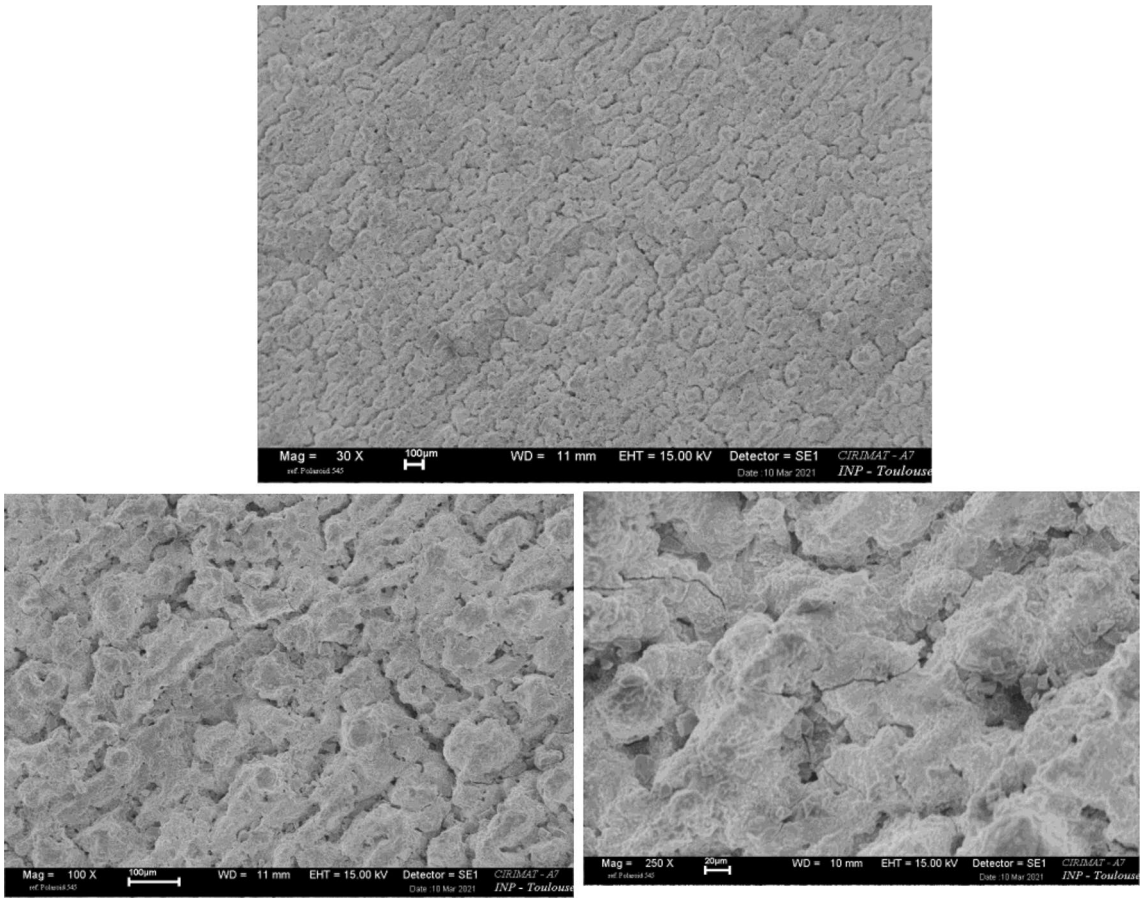

Fig. 11 SiC part manufactured by PBSLP. The laser power, the scanning speed, the layer thickness, the hatching distance, the scanning strategy, and the powder compaction were 45 W, 250 mm/s, 30 µm, 35 µm, hexagonal rotated by 90 degrees between layers and 100%

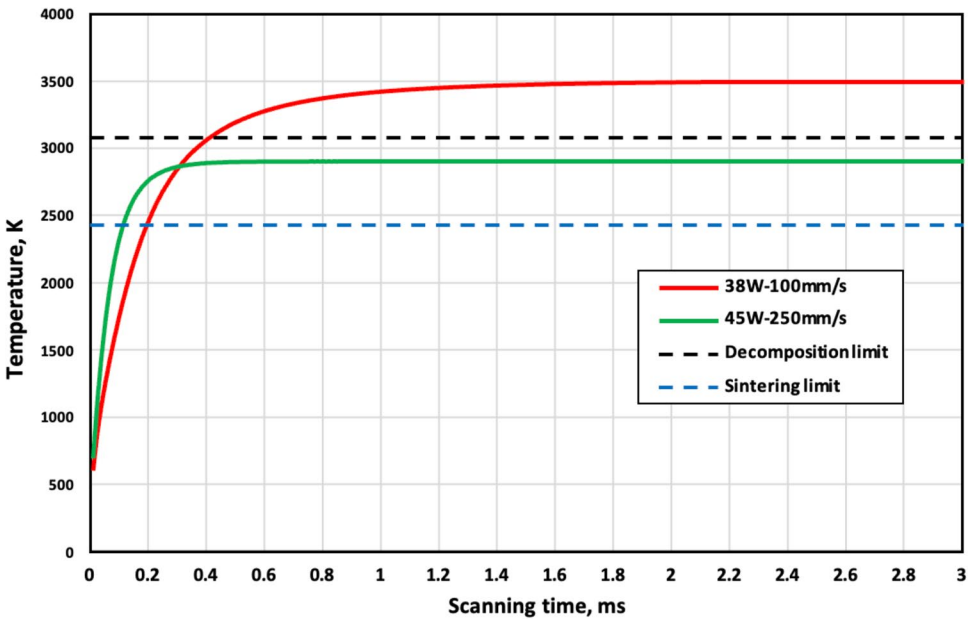

Fig. 12 Temperature history for 45 W-250 mm/s and 38 W-100 mm/s cases

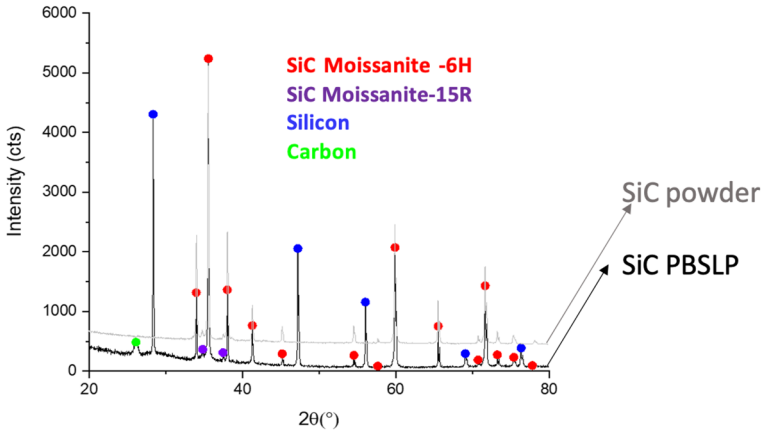

Fig. 13 XRD spectra of the SiC powder and SiC manufactured part by PBSLP

Table 6 Phase composition determined by Rietveld method [25] of XRD patterns of SiC powder and SiC 3D part samples prepared by PBSLP

Sample	Name	SiC-6H	SiC-15R	Silicon	Carbon	Rwp (%)	Rexp (%)
SiC powder	As- received	96.65% ± 1.30	3.35% ± 0.47	–	–	14.23	3.05
SiC 3D part	After PBSLP	91.85% ± 2.31	1.89% ± 0.39	5.21% ± 0.20	1.04% ± 0.28	22.19	4.23

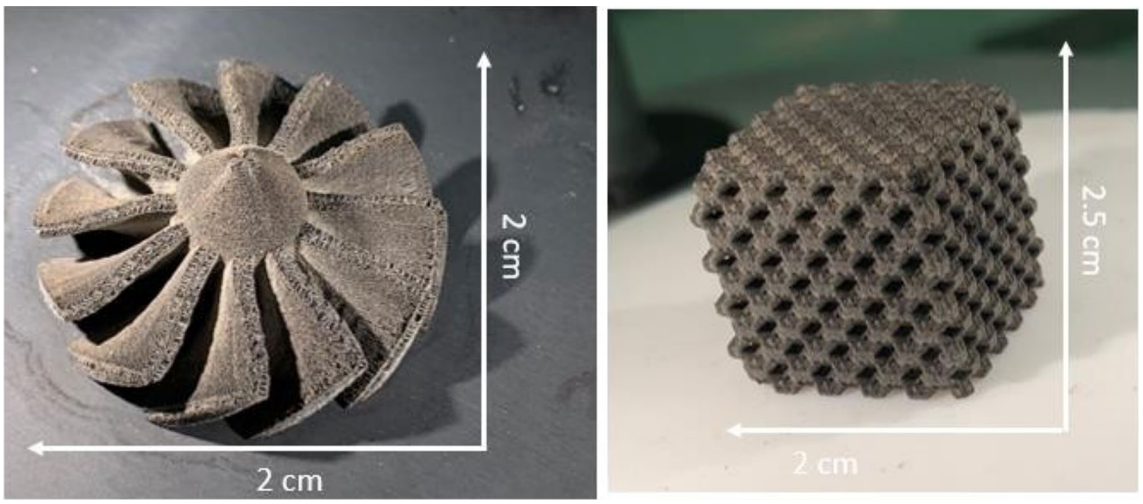

Fig. 14 SiC turbine and SiC lattice structure manufactured with PBSLP

Table 7 Comparison of SiC relative density manufactured by PBSLP

Ref	Feedstock	PBSLP Relative density samples prior post-treatment
This work	SiC powder	81%
Meyers et al. [16]	Si 40% vol. + SiC 60% vol	54%
Liu et al. [12]	Formaldehyde resin (18% wt.) + SiC	41%
Jin et al. [13]	SiC + epoxy resin (3% wt.)	47%
Song et al. [15]	SiC + spheroidal- graphite + coarse silicon particles + Epoxy resin + Dicyandiamide	45%

[a]Includes 6 cycles of Polycarbosilane Infiltration Pyrolisis

Finally, comparing the results obtained in this work with other recent investigation using PBSLP as a manufacturing technique for SiC (Table 7), a much higher relative density (≥27%) of the final SiC manufactured parts prior post-treatments is reached. In general, this difference is achieved since published works focus on the optimization of laser power and scanning speed without due optimization of other parameters, such as hatching distance, layer thickness, scanning strategy, and powder compaction. Moreover, even though the use of different initial powder mixtures or binders, such as Silicon or epoxy resin, solve the lack of the SiC melt phase under normal atmospheric circumstances to bond the powder particles together, during the PBSLP process, the reached temperature is not sufficient to sinter the silicon carbide, therefore, the density of the manufactured parts is much lower.

6 Conclusion

Silicon carbide parts were manufactured by means of D-PBSLP in the absence of post-treatments and any addition of additives in the initial powder mixture. The optimization of the parameters process was performed by numerical and experimental analysis. The numerical model was used to determine the effect of laser power, scanning speed, layer thickness and hatching distance. Following the numerical results, the optimal process parameters were set at laser power: 45 W, scanning speed: 250 mm/s, layer thickness: 30 µm, hatching distance: 35 µm, scanning strategy: hexagonal rotated by 90° between layers and compaction: 100%, respectively. Final SiC parts exhibit 81% of relative density and 5 and 1% of residual Silicon and Carbon, respectively, which corresponds to some decomposition during the process due to high temperature peaks inherently generated by the scanning strategy. In consequence, this paper proves the viability of the D-PBSLP as a shaping technique to manufacture SiC 3D parts.Moreover, the process viability was confirmed with the manufacturing of SiC complex shapes, specific, SiC lattice structures that cannot be obtained with traditional manufacturing techniques.

Author Contribution Alejandro Montón Zarazaga and Mohammed Abdelmoula performed the experimental and numerical study for Direct Selective Laser Sintering of Silicon Carbide and wrote the manuscript. All authors read and approved the final manuscript.

Funding This project has received funding from the European Union's Framework Program for Research and Innovation Horizon 2020 (2014–2020) under the Marie Skłodowska-Curie Grant Agreement No. [764935].

Availability of data and material The authors confirm that the data supporting the findings of this study are available within the article and/or its supplementary materials.

Code availability The authors confirm that the code is available upon request.

Declarations

Conflict of interest The authors declare that they have no conflict of interest/competing interests.

Ethical Approval All applicable international, national, and/or institutional guidelines for the care and use of research and materials were followed.

Consent to Participate Not applicable.

Consent for publication Authors give the Publisher the permission to publish the Work.

References

1. Kimoto T, Cooper JA (2014) Fundamentals of silicon carbide technology: growth, characterization, devices, and applications. Wiley, Singapore
2. Ohji T, Singh M, Halbig M (2015) Advanced processing and manufacturing technologies for nanostructured and multifunctional materials II: a collection of papers presented at the 39th International Conference on Advanced Ceramics and Composites. Wiley, Hoboken
3. Leray C, Ferriere A, Toutant A, Olalde G, Peroy J, Chéreau P, Ferrato (2017) Design and proof of concept of an innovative very high temperature ceramic solar absorber. Abu Dhabi, United Arab Emirates, p 030032. https://doi.org/10.1063/1.4984375
4. Bougoin M, Mallet F, Lavenac J (2019) Full-SiC EUCLID's very large telescope. In: Karafolas N, Sodnik Z, Cugny B (eds) International Conference on Space Optics — ICSO 2018. SPIE, Chania, Greece, p 60
5. Bougoin M, Coatantiec C, Lavenac J, Costes V (2017) A new technological step for sic mirrors preparing OTOS. In: Cugny B, Sodnik Z, Karafolas N (eds) International Conference on Space Optics — ICSO 2014. SPIE, Tenerife, Canary Islands, Spain, p 38
6. Castel D, Sein E, Lopez S (2012) The 3.2m all SiC telescope for SPICA. In: Navarro R, Cunningham CR, Prieto E (eds) Modern technologies in space- and ground-based telescopes and instrumentation II. Society of Photo-Optical Instrumentation Engineers (SPIE) Conference Series. Amsterdam, p 84502
7. Cai K, Román-Manso B, Smay JE, Zhou J, Osendi MI, Belmonte M, Miranzo P et al (2012) Geometrically complex silicon carbide structures fabricated by robocasting. J Am Ceram Soc 95:2660–2666. https://doi.org/10.1111/j.1551-2916.2012.05276.x

8. Bai X, Ding G, Zhang K, Wang W, Zhou N, Fang D, He R (2021) Stereolithography additive manufacturing and sintering approaches of SiC ceramics. Open Ceram 5:100046. https://doi.org/10.1016/j.oceram.2020.100046
9. Gonzalez JA, Mireles J, Lin Y, Wicker RB (2016) Characterization of ceramic components fabricated using binder jetting additive manufacturing technology. Ceram Int 42:10559–10564. https://doi.org/10.1016/j.ceramint.2016.03.079
10. Grossin D, Montón A, Navarrete-Segado P et al (2021) A review of additive manufacturing of ceramics by powder bed selective laser processing (sintering / melting): Calcium phosphate, silicon carbide, zirconia, alumina, and their composites. Open Ceram 5:100073. https://doi.org/10.1016/j.oceram.2021.100073
11. He R, Zhou N, Zhang K, Zhang X, Zhang L, Wang W, Fang D (2021) Progress and challenges towards additive manufacturing of SiC ceramic. J Adv Ceram 10:637–674. https://doi.org/10.1007/s40145-021-0484-z
12. Liu K, Wu T, Bourell DL, Tan Y, Wang J, He M, Sun H, Shi Y, Chen J (2018) Laser additive manufacturing and homogeneous densification of complicated shape SiC ceramic parts. Ceram Int 44:21067–21075. https://doi.org/10.1016/j.ceramint.2018.08.143
13. Jin L, Zhang K, Xu T, Zeng T, Cheng S (2018) The fabrication and mechanical properties of SiC/SiC composites prepared by SLS combined with PIP. Ceram Int 44:20992–20999. https://doi.org/10.1016/j.ceramint.2018.08.134
14. Chen F, Liu K, Sun H, Shui Z, Liu C, Chen J, Shi Y (2018) Fabrication of complicated silicon carbide ceramic components using combined 3D printing with gelcasting. Ceram Int 44:254–260. https://doi.org/10.1016/j.ceramint.2017.09.166
15. Song S, Gao Z, Lu B, Bao C, Zheng B, Wang L (2019) Performance optimization of complicated structural SiC/Si composite ceramics prepared by selective laser sintering. Ceram Int. https://doi.org/10.1016/j.ceramint.2019.09.004
16. Meyers S, De Leersnijder L, Vleugels J, Kruth J-P (2018) Direct laser sintering of reaction bonded silicon carbide with low residual silicon content. J Eur Ceram Soc 38:3709–3717. https://doi.org/10.1016/j.jeurceramsoc.2018.04.055
17. Birmingham BR, Marcus HL (1995) Solid freeform fabrication of silicon nitride shapes by selective laser reaction sintering (SLRS). SFF Symposium, Texas
18. Hon KKB, Gill TJ (2003) Selective laser sintering of SiC/polyamide composites. CIRP Ann 52:173–176. https://doi.org/10.1016/S0007-8506(07)60558-7
19. Löschau W, Lenk R, Scharek S (2000) Prototyping of complex-shaped parts and tools of Si/SiC-ceramics. Ind Ceram 38:6. https://doi.org/10.1002/3527607293.ch24
20. Regenfuss P, Streek A, Hartwig L, Klötzer S, Brabant T, Horn M, Ebert R, Exner H (2007) Principles of laser micro sintering. Rapid Prototyp J 13:204–212. https://doi.org/10.1108/13552540710776151
21. Streek A, Regenfuss P, Ebert R, Exner H (2009) Laser micro sintering - upgrade of the technology. In: Proceedings of the ICALEO conference, Orlando, FL, USA
22. Meyers S, Leersnijder LD, Vleugels J, Kruth J-P (2018) Increasing the silicon carbide content in laser sintered reaction bonded silicon carbide. In: Bansal NP, Castro RHR, Jenkins M et al (eds) Ceramic transactions series. Wiley, Hoboken, pp 207–215
23. Meyers S (2019) Additive manufacturing of technical ceramics. PhD thesis, KU Leuven University, Belgium
24. Montón A, Abdelmoula M, Küçüktürk G, Grossin D, Maury F, Ferrato M (2021) Experimental and numerical study for direct powder bed selective laser processing (sintering/melting) of silicon carbide ceramic. Mater Res Express 8:045603. https://doi.org/10.1088/2053-1591/abf6fc
25. Abdelmoula M, Zarazaga AM, Küçüktürk G, Grossin D, Maury F, Ferrato M et al (2022) Scanning strategy investigation for direct powder bed selective laser processing of silicon carbide ceramic. Appl Sci 12:788. https://doi.org/10.3390/app12020788
26. Yablokova G, Speirs M, Van Humbeeck J, Kruth JP, Schrooten J, Cloots F, Boschini F, Lumay G, Luyten J (2015) Rheological behavior of β-Ti and NiTi powders produced by atomization for SLM production of open porous orthopedic implants. Powder Technol 283:199–209. https://doi.org/10.1016/j.powtec.2015.05.015
27. Spierings AB, Voegtlin M, Bauer T, Wegener K (2016) Powder flowability characterisation methodology for powder-bed-based metal additive manufacturing. Prog Addit Manuf 1:9–20. https://doi.org/10.1007/s40964-015-0001-4
28. Navarrete-Segado P, Frances C, Grossin D, Tourbin M (2022) Tailoring hydroxyapatite microspheres by spray-drying for powder bed fusion feedstock. Powder Technol 398:117116. https://doi.org/10.1016/j.powtec.2022.117116
29. Hongchao L, Changlin K (1997) Quantitative analysis of SiC polytype distributions by the Rietveld method. J Mater Sci 32:2661–2664. https://doi.org/10.1023/A:1018623122324
30. Moser D, Fish S, Beaman J, Murthy J (2014) Multi-layer computational modeling of selective laser sintering processes. In: Volume 2A: advanced manufacturing. american society of mechanical engineers: Montreal, p V02AT02A008
31. Groth R, Kauer E (1961) Absorption freier Ladungsträger in α-SiC-Kristallen. Phys Status Solidi B 1:445–450. https://doi.org/10.1002/pssb.19610010504
32. Suzuki A, Nishida R, Takata N, Kobashi M, Kato M (2019) Design of laser parameters for selectively laser melted maraging steel based on deposited energy density. Addit Manuf 28:160–168. https://doi.org/10.1016/j.addma.2019.04.018